PCCP

PAPER

Cite this: *Phys. Chem. Chem. Phys.*, 2018, **20**, 2797

Combining experimental and modelling approaches to study the sources of reactive species induced in water by the COST RF plasma jet†

Y. Gorbanev, *[a] C. C. W. Verlackt,[a] S. Tinck,[a] E. Tuenter,[b] K. Foubert,[b] P. Cos[b] and A. Bogaerts *[a]

Received 11th November 2017,
Accepted 5th January 2018

DOI: 10.1039/c7cp07616a

rsc.li/pccp

The vast biomedical potential of cold atmospheric pressure plasmas (CAPs) is governed by the formation of reactive species. These biologically active species are formed upon the interaction of CAPs with the surroundings. In biological milieu, water plays an essential role. The development of biomedical CAPs thus requires understanding of the sources of the reactive species in aqueous media exposed to the plasma. This is especially important in case of the COST RF plasma jet, which is developed as a reference microplasma system. In this work, we investigated the formation of the OH radicals, H atoms and H_2O_2 in aqueous solutions exposed to the COST plasma jet. This was done by combining experimental and modelling approaches. The liquid phase species were analysed using UV-Vis spectroscopy and spin trapping with hydrogen isotopes and electron paramagnetic resonance (EPR) spectroscopy. The discrimination between the species formed from the liquid phase and the gas phase molecules was performed by EPR and ^{1}H-NMR analyses of the liquid samples. The concentrations of the reactive species in the gas phase plasma were obtained using a zero-dimensional (0D) chemical kinetics computational model. A three-dimensional (3D) fluid dynamics model was developed to provide information on the induced humidity in the plasma effluent. The comparison of the experimentally obtained trends for the formation of the species as a function of the feed gas and effluent humidity with the modelling results suggest that all reactive species detected in our system are mostly formed in the gas phase plasma inside the COST jet, with minor amounts arising from the plasma effluent humidity.

Introduction

Cold atmospheric pressure plasmas (CAPs) have attracted a lot of attention due to their vast potential in biomedical applications.[1–3] CAPs have been used to modify or produce surfaces with high bacterial resistance, used in medicinal applications.[4,5] They have also been applied in dentistry (including teeth whitening)[4,6] and in sterilisation processes.[7] In recent years, CAPs have been demonstrated to efficiently deactivate bacteria,[2,8] viruses,[9] and cancer cells,[2,10–12] and facilitate healing of chronic wounds.[2,13]

As a result of the extensive research work, a plethora of plasma devices has been reported.[13–15] Most common CAP devices used in biomedical research are atmospheric pressure plasma jets.[13,16] They enable direct treatment of biological substrates due to their main properties: ambient temperature, feed gas flow for a targeted delivery of the biologically active species, minimised electrical impact, *etc.* A plasma jet is operated with a flow of gas between the electrodes. This feed gas is usually an inert gas (Ar or He, with or without admixtures[16]), although the use of N_2 or air in plasma jets has also been reported.[17,18] The reactive oxygen and nitrogen species (RONS), which are responsible for the biomedical effects of CAPs, may be generated inside the jet (*e.g.*, when plasma contains air), or upon interaction of the plasma effluent with the ambient atmosphere (when plasma contains inert gases only).[1,3,16] Other plasma parameters are the type of discharge (pulsed or continuous sinusoidal), frequency (MHz, kHz), electrode configuration, *etc.*[3,14,18] Based on the type of electrode configuration, parallel field and cross field plasma jets are distinguished, with the feed gas flowing parallel or perpendicular to the applied electric field, respectively. When a cross field plasma jet is used, most of the charged species (ions and electrons) are confined within the area between the electrodes, and the effluent largely consists of neutral species (radicals and metastable excited species). The combination of the plasma parameters has a dramatic effect on the processes leading to the formation of the reactive species.[1,3]

[a] *Research Group PLASMANT, Department of Chemistry, University of Antwerp, Campus Drie Eiken, Universiteitsplein 1, Wilrijk, Antwerpen, BE-2610, Belgium. E-mail: yury.gorbanev@uantwerpen.be, annemie.bogaerts@uantwerpen.be*
[b] *Department of Pharmaceutical Sciences, University of Antwerp, Campus Drie Eiken, Universiteitsplein 1, Wilrijk, Antwerpen, BE-2610, Belgium*

† Electronic supplementary information (ESI) available: Description of the 3D fluid dynamics model and further experimental data. See DOI: 10.1039/c7cp07616a

The COST radio frequency (RF) plasma jet was introduced within an EU COST action as a reference microplasma jet to establish a comparison standard between different research groups, as shown by Golda *et al.*[19] Its scalability and reproducibility (including modifications) has led to various uses in both industry-oriented[20,21] and biomedical research.[11] The COST RF plasma jet is a cross field jet, usually operated with helium or argon as a feed gas (neat or with introduced admixtures). A computational model of the chemical kinetics has been developed for the gas phase plasma of such jet by Murakami *et al.*[22,23] Experimentally, the COST jet has been studied using optical methods (optical emission spectroscopy,[19] laser-induced fluorescence,[24] UV[25] and cavity ring-down laser[26] absorption spectroscopy, *etc.*) and mass spectrometry,[27] thus benchmarking the model and providing information on the concentrations of RONS in the gas phase plasma.

We have previously reported a deactivation of melanoma and glioblastoma cancer cells in solutions exposed to the COST jet.[11] Liquid water is an essential part of the biological milieu, making the study of the reactive species induced in water by plasma crucial for the applied research.[28] Recently, Hefny *et al.* have identified several reactive species in aqueous solutions in contact with the COST jet.[29] The authors have specifically demonstrated that the jet is capable of producing biologically relevant reactive oxygen species (ROS), such as oxygen atoms, and delivering them into the exposed liquid samples. However, the origin of other reactive species is still not fully described. Gaining insights into the origin of the ROS and the factors governing their formation is required for a more complete understanding of this jet.

The nature, amount and the source of the species detected in the liquid depends largely on the type of the plasma jet. For example, Takamatsu *et al.* suggested that in the plasma setup used in their work the radical species were at least partially formed inside the liquid water.[30] On the other hand, Xu *et al.* proposed that in their work ROS were initially formed in the gas phase, followed by their delivery to the exposed liquid.[31] Similarly, using a kINPen plasma jet, Winter *et al.* correlated the liquid phase concentration of H_2O_2 with the feed gas humidity,[32] although recent model calculations show that in certain cases ROS can be produced directly in the liquid.[10,33]

Previously, we have demonstrated that a sinusoidal kHz-frequency parallel field plasma jet generated reactive oxygen species (ROS) in the gas phase.[34] These species are further delivered to the liquid which is in contact with the plasma jet effluent. This was determined *via* a method we have developed to distinguish between the ROS produced in the gas and the liquid phase.

In this work, we combined experimental and computational studies to investigate the source of the reactive species in aqueous solutions exposed to the COST jet. We investigated the effects of varied amounts of water vapour introduced in the feed gas and in the plasma effluent on the concentrations of the formed reactive species (H, OH, H_2O_2). For the first time, a combination of experimental techniques, including the use of isotopically labelled water, zero-dimensional (0D) chemical kinetics modelling of the gas phase plasma and three-dimensional (3D) fluid dynamics modelling of the gas inside the reactor was used. The obtained results provide valuable insights in the sources of the studied reactive species.

Experimental

Materials

Deuterium oxide D_2O (99.9 atom% D), hydrogen peroxide H_2O_2 (30%), 4-hydroxy-2,2,6,6-tetramethylpiperidine 1-oxyl (4-hydroxy-TEMPO) (97%), potassium titanium oxide oxalate dihydrate $K_2TiO(C_2O_4)_2{\cdot}2H_2O$ ($\geq$98%), *N-tert*-butyl-α-phenylnitrone (PBN) ($\geq$98%), sulphuric acid H_2SO_4 (95–97%) and sodium *p*-toluenesulfonate (sodium tosylate) $CH_3C_6H_4SO_3Na$ (95%) were purchased from Sigma-Aldrich. 5,5-Dimethyl-1-pyrroline *N*-oxide (DMPO) ($\geq$99%) was obtained from Dojindo Molecular Technologies, Inc. Helium He (99.999%) was supplied by Praxair.

De-ionised water was used for the preparation of the solutions. All chemicals were used as received.

Plasma setup

For the experiments, the COST RF plasma jet was used (Fig. 1). A detailed description of the characteristics of the COST RF jet can be found elsewhere.[19] The plasma was ignited in a rectangular cuboid cavity (30 mm × 1 mm × 1 mm) between two electrodes. The electrodes and the cavity were covered with quartz glass. A Pico Technology PicoScope PC Oscilloscope voltage probe was used to measure the time-resolved root mean square voltage (V_{RMS}). In all experiments, the plasma was sustained at 250 V_{RMS} and at an operating frequency of 13.56 MHz. The plasma jet and the exposed liquid sample were positioned inside a glass reactor.

The plasma was operated with a feed gas of helium with water admixtures controlled by mass flow controllers (MFCs) equipped with a microcomputer controller (Brooks Instruments 0254). The highest water content (per cent of relative saturation) of the feed gas was 35%. This was the largest water admixture at which it was possible to reach the plasma ignition. All experiments were carried out with a total feed gas flow rate of 1 L min^{-1}.

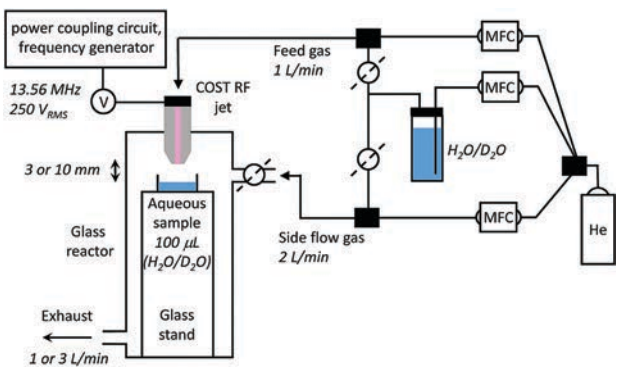

Fig. 1 Schematic plasma setup of the COST RF jet with an in-house built glass reactor to control the gaseous environment. The split He flow was used either for the feed gas or the side flow He.

In experiments involving a side flow of gas, the total side flow rate of the gas was 2 L min^{-1}, being either dry He or with water vapour admixtures (20–100% saturation). The concentration of water vapour is quoted in per cent of the saturation at 21–22 °C (ambient temperature during the experimental work). All temperature measurements were performed with an Extech Instruments TM100 thermometer.

Prior to the experiments, the system was flushed with dry He for 60 min.

Analysis

Electron paramagnetic resonance (EPR) measurements were carried out on a Magnettech MiniScope MS 200 spectrometer. The EPR analysis parameters were as follows: frequency 9.4 GHz, power 5 dBm (3.16 mW), modulation frequency 100 kHz, modulation amplitude 0.1 mT, sweep time 40 s, time constant 0.1, sweep width 10 mT, number of scans 3. For the measurements, the analysed samples were contained in 50 μL glass capillaries (Hirschmann). The concentrations reported were obtained *via* double integration of the respective simulated spectra of the formed nitroxide radical adducts. The simulations were performed using a NIEHS P.E.S.T. WinSIM ver. 0.96 using the hyperfine values obtained from literature.[35] EPR calibration was performed using aqueous solutions of a stable radical 4-hydroxy-TEMPO in a range of concentrations 5–500 μM (Fig. S1 in ESI†). After each plasma exposure experiment, the samples were immediately placed in a capillary tube. The overall time between the exposure and spectrum recording was 1 minute.

The concentration of H_2O_2 in the liquid samples was determined by UV-Vis measurements performed on a ThermoFischer Genesys 6 spectrophotometer. Quartz cuvettes were used with a 10 mm path length (internal width 2 mm) and a volume of 700 μL. UV-Vis calibration was done using 100 μL of the titanium reagent with added 200 μL of aqueous hydrogen peroxide solutions in a range of concentrations 0.2–2 mM (ESI,† Fig. S1). Titanium(IV) reagent was prepared by dissolving 0.354 g of $K_2TiO(C_2O_4)_2{\cdot}2H_2O$ in a mixture of 2.72 mL of sulphuric acid and 3 mL of H_2O, and diluting the resulting solution with H_2O to a total volume of 10 mL. UV-Vis spectra of the samples were recorded as follows. 60 μL of plasma-exposed sample (immediately after exposure) were mixed with 140 μL of H_2O and 100 μL of the titanium reagent, and then incubated for 2 min before the measurement. The concentration of H_2O_2 was determined from the intensity of the peak at 400 nm.

The composition of the D_2O samples was analysed by ^{1}H-NMR with added external standard. 50–60 μL of plasma-exposed sample was added to 500–600 μL of 0.47 M $CH_3C_6H_4SO_3Na$ solution in D_2O in a Young NMR tube and kept under nitrogen. Sodium tosylate was pre-dried before the dissolution in D_2O. The weight of the analyte and the sodium tosylate solution was monitored using a high precision laboratory balance. The NMR spectra were recorded on a Bruker DRX-400 instrument, operating at 400 MHz for quantitative ^{1}H analysis with a 30° flip angle and a delay D1 of 10 s. The spectra were analysed using MestReNova ver. 11.0. The H_2O content of the D_2O samples is quoted after correction for the H_2O present in the external standard. The dissolution of spin traps or sodium tosylate in D_2O did not increase its water content. Handling the sample under the experimental conditions resulted in an increase of the H_2O content of the liquid sample from 0.1 to 0.4 mol% (see Table S1 in the ESI†).

The concentrations of all measured reactive species in the liquid samples are quoted after correction for the evaporation of the solvent during the experiment. The extent of the evaporation (*i.e.*, the volume of the evaporated sample) was assessed by weighing the liquid sample before and after the plasma exposure. The corrected concentration values were obtained as show in eqn (1). C is the

$$C_{\text{corrected}} = C_{\text{experimental}} \cdot \frac{V_{\text{after exposure}}}{V_{\text{before exposure}}} \quad (1)$$

concentration of a reactive species, and V is the volume of the liquid sample. All data points shown in the figures are averaged for three measurements. The error bars shown in the figures are standard deviations of these measurements. The results of the ^{1}H-NMR analysis are an average of two experiments. The standard deviation values did not exceed 14% (not shown).

Plasma exposure experiments

In a typical experiment, 100 μL of liquid sample was placed in a well on top of a glass stand inside the glass reactor. The sample surface was positioned at either 3 or 10 mm from the plasma jet nozzle. The reactor was closed and flushed with the feed gas (He with 0–35% water saturation) for 20 s and then exposed to plasma for 60 s. In the experiments with the side flow of gas into the reactor (He with 0–100% water saturation), the plasma feed gas was dry He.

For the spin trapping experiments, a 100 mM solution of a spin trap (DMPO or PBN) was prepared in H_2O or D_2O. To elucidate the possibility of rapid radical adduct decay within the experimental time scale[36] which may affect the observed trends, 100 mM solution of the PBN spin trap was treated by plasma under different experimental conditions. In all cases the concentration of the formed radical adduct increased with the treatment time (ESI,† Fig. S2).

The experiments involving different feed gas humidity were performed by using a split helium flow (see Fig. 1). The dry He gas was mixed with He saturated with H_2O or D_2O in different proportions. H_2O/D_2O saturation of helium was achieved by passing dry helium through a Drechsel flask filled with H_2O or D_2O at 21–22 °C, as described elsewhere.[34]

Computational models

Three-dimensional (3D) fluid dynamics model

A 3D fluid dynamics model was developed to investigate the flow of both the feed gas and side flow gas of the system. This model combines two physical modules.

(1) Transport of momentum is governed by the compressible and time-independent Navier–Stokes eqn (2) and (3). These expressions represent the conservation of mass and momentum,

respectively. ρ is the overall mass density, $\vec{u}$ is the fluid velocity, μ is the dynamic viscosity, p is the static pressure, and I represents a unity matrix.

(2) Transport of mass, which is affected by diffusion and convection (eqn (4)). c_i and D_i are the concentration and diffusion coefficient of each species i. R_i is the sum of all production and loss terms in the simulation, which in our case are the inlet and the exhaust of the reactor. The left side of the equation represents changes in concentration due to diffusion (governed by D_i) and convection (see velocity $\vec{u}$).

$$\rho\nabla\cdot\vec{u} = 0 \quad (2)$$

$$\rho(\vec{u}\cdot\nabla\vec{u}) = \nabla\left[-pI + \mu\left(\nabla\vec{u} + (\nabla\vec{u})^{\mathrm{T}}\right) - \frac{2}{3}\mu(\nabla\cdot\vec{u})I\right] \quad (3)$$

$$\nabla\cdot(-D_i\nabla c_i) + \vec{u}\cdot\nabla c_i = R_i \quad (4)$$

Two geometries were considered with different gaps between the plasma jet and the liquid. In practice, this means that the plasma jet was moved in the Z-direction (*i.e.* height) in such a way that the distance between the nozzle of the jet and the surface of the liquid was either 3 or 10 mm. The geometry is described in more detail in Fig. S3 in the ESI.†

Zero-dimensional (0D) chemical kinetics model

In the 0D chemical kinetics model (ZDPlaskin), the balance equations for the different plasma species are solved, based on production and loss terms.[37] Such 0D model allows for the use of a very detailed and extensive reaction set with about 2000 reactions, within a reasonable calculation time. The chemistry set for humid air was adopted from our previous work (Van Gaens *et al.*[38]), while He reactions with air (to include the N_2 and O_2 impurities in commercial He‡) were used as reported by Murakami *et al.*[22,23] In our simulations, we considered 134 species, which react with each other in 1725 chemical reactions, including electron impact reactions, ion and neutral reactions.

The ZDPlaskin code also contains a built-in Boltzmann solver (BOLSIG+)[39] used to calculate the electron energy distribution function and electron impact rate coefficients based on a set of cross sections adopted from literature.[22,38]

In the model, a constant axial flow speed in the jet is considered, which is realistic for the investigated conditions. This allowed us to correlate the calculated time-dependence of the species densities within ZDPlaskin with the transport of the gas through the plasma jet. Thus, we obtained information on the species densities as a function of position both inside and outside (*i.e.*, effluent) of the plasma jet (see detailed description of this approach in Van Gaens *et al.*[38]). In the effluent, the flow speed was gradually decreased to 30% of the initial flow speed at a distance of 10 mm away from the plasma jet, based on flow data of the 3D fluid dynamics model. The initial gas temperature was defined in the model as 21.5 °C. The temperature then gradually increased to 50 °C (near the end of the plasma jet), after which it cools down to 35 °C at 10 mm into the effluent. Although we have not measured the temperature of the plasma jet, these values were reasonable for the COST RF jet.[40] We have also performed calculations for 'envelope' conditions (*i.e.*, different temperature), which showed little differences for the species density.§ In any case, in this work we compare not the absolute values, but the trends of the species concentrations. Other operating conditions, such as power deposition, gas composition and pressure, correspond to the experimental conditions.

‡ The commercial He gas contained H_2O (3 ppm), N_2 (5 ppm), O_2 (2 ppm) and H_2 (1 ppm) impurities, as reported by the supplier.

Results and discussion

Fluid dynamics and delivery of species from the gas phase into the liquid

We used a reactive system which allowed to exclude ambient air (containing uncontrollable amounts of H_2O vapour) from being in contact with the COST RF plasma jet.[41] This was achieved by using a dedicated glass reactor that encapsulated the plasma jet, the effluent, and the liquid sample (Fig. 1). The COST jet was in direct contact with the liquid inside the reactor. The gaseous mixture inside the reactor consisted of the feed gas components and the evaporated sample. In some experiments, an additional gas was introduced into the reactor with the side flow of gas. This was aimed at studying the effect of the humidity specifically in the effluent on the formation of reactive species.

As mentioned above, the experiments were performed for two distances (gaps) between the plasma jet nozzle and the surface of the liquid sample, *i.e.*, 3 and 10 mm. This was done to demonstrate the difference with respect to the species originating in the gas phase plasma. The 10 mm distance was chosen as a larger gap, but it was checked that the gas flow from the plasma jet to the liquid sample was undisturbed by the side flow of 2 L min^{-1}, as estimated by the 3D fluid dynamics model (Fig. 2). The average velocity of the side flow (2 L min^{-1}) was 1.3 m s^{-1}, compared to 14.2 m s^{-1} found in the effluent, and it had no impact on the plasma effluent flow itself (see Fig. S4 in the ESI†). This is also clear from the direction of the flow depicted in Fig. 2 (indicated by black arrows). Thus, despite the presence of the side flow, the gas flow from the plasma jet remained undisturbed.

We have previously shown that some reactive species (*e.g.*, H_2O_2, O_3) may be formed inside the plasma jet, and not in the effluent.[34] The effectiveness of introducing these species into the liquid sample critically depends on the gas phase dynamics and the diffusion of these species into the liquid. Thus, another important factor analysed by the fluid dynamics modelling was the concentration of species (on the example of water molecules) brought towards the liquid surface by the gas flow. This was done by modelling the conditions when He feed gas was with 5 or 35% H_2O saturation in the absence of the side flow. The results are presented in Table 1.

§ The 'envelope' conditions for the simulations were as follows: (i) 21.5 °C inlet, raising to 150 °C in the reactor, decreasing to 100 °C in the effluent; (ii) constant temperature 21.5 °C. The deviation of H_2O_2, OH and H densities from those reported in our work was *ca.* 5% and 1%, for (i) and (ii), respectively, while the trends remained the same (not shown).

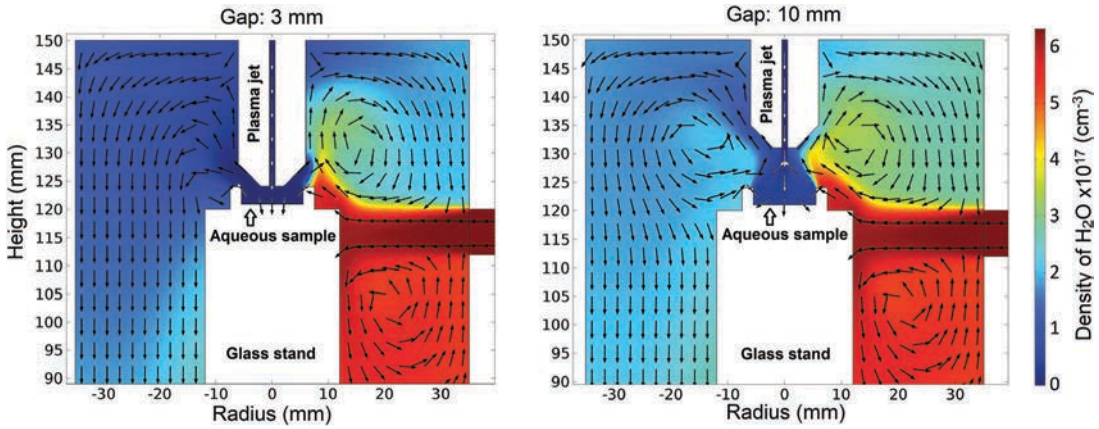

Fig. 2 Two-dimensional (2D) cross section of the fluid dynamics model results of the H_2O density. The cross section is taken through the centre of the glass reactor, parallel with the plasma jet and the inlet/exhaust of the reactor. Results are shown for 3 mm and 10 mm gap between the plasma jet nozzle and the liquid sample. With each gap, the modelling results are shown for the following conditions: dry He feed gas with 100% H_2O–saturated He side flow. The H_2O density is plotted in cm^{-3} and indicated with a colour legend. The direction of the flow is shown with black arrows.

Table 1 Concentration of H_2O above the liquid surface as predicted by the 3D fluid dynamics model

Entry	Gap[a] (mm)	H_2O vapour saturation of the gas		Concentration of H_2O above the liquid surface[d] (μmol L^{-1})
		% saturation[b]	μmol L^{-1} [c]	
5 or 35% H_2O–saturated He feed gas with no side flow gas				
1	10	5	52.4	52.3
2	10	35	367.1	367.0
3	3	5	52.4	52.4
4	3	35	367.1	367.1
Dry He feed gas with 20, 50 or 100% H_2O–saturated side flow gas				
5	10	20	209.8	11.7
6	10	50	524.4	29.3
7	10	100	1048.9	58.5
8	3	20	209.8	0.3
9	3	50	524.4	0.8
10	3	100	1048.9	1.6

[a] Distance from the plasma jet nozzle to the liquid surface. [b] Achieved by splitting the He flow. [c] Values obtained from literature for H_2O vapour saturation at 21.5 °C. [d] Values of H_2O concentration brought into the effluent by the feed gas and/or the side flow gas, as obtained from the 3D fluid dynamics modelling.

The concentration of water was the same in the cases of 3 and 10 mm (Table 1, entries 1–4), indicating the equally efficient delivery of species (*i.e.*, H_2O molecules) from inside the jet to the surface of the liquid, with minimal dissipation into the reactor.

The diffusion of the H_2O vapour from the side flow gas into the effluent was also assessed using the 3D fluid dynamics model (as shown in Fig. 2). At the 10 mm gap, the H_2O content (coming in the effluent from the side flow gas) was substantially higher than at 3 mm (Table 1, entries 5–10). Even with a 100% H_2O–saturated side flow gas, the H_2O concentration above the liquid was negligible: 1.6 μmol L^{-1} (entry 10). For comparison, with a gap of 10 mm this concentration was 58.5 μmol L^{-1} (entry 7). This clearly indicated that practically no diffusion from the side flow gas into the effluent occurred at 3 mm, while its effect is clearly seen at 10 mm. At distances shorter than 3 mm, the liquid sample was significantly perturbed by the high velocity gas flow of the plasma jet, as observed in the experiments, thus making the 3 mm distance pertaining to the experiments.

Further, we experimentally investigated the delivery of species from the plasma into the aqueous sample positioned at these two different distances from the plasma jet nozzle (3 and 10 mm). The use of isotopically labelled water enabled distinguishing between the water present in the liquid state and coming from the gas phase. In the experiments, a 100 μL sample of D_2O was positioned inside the reactor and exposed to the COST RF plasma jet. The ^{1}H-NMR analysis with sodium *p*-toluenesulfonate as an external standard allowed to estimate the amounts of H_2O induced in the liquid sample by the gas (Table 2). We note that the presented values correspond to 1 min of plasma exposure. At any moment during the exposure, the molar fraction of H_2O in D_2O was lower.

As seen from the results, the amount of H_2O delivered to the D_2O sample after exposure to the COST jet increased with increasing H_2O amount in the gas phase, as expected. It was virtually the same at 3 and 10 mm (Table 2, entries 1–4 and 6–9), which agreed well with the fluid dynamics simulation results (Table 1, entries 1–4). In the case of the side flow of He, even at 100% H_2O–vapour saturation a minor amount (*ca.* 3%) of H_2O was brought into the liquid at the 10 mm distance (Table 2, entry 12), with only a negligible amount at 3 mm (Table 2, entry 13). This was also in good agreement with the fluid dynamics computational results discussed above (see Table 1, entries 5–10). For comparison, a 100% H_2O–saturated feed gas resulted in the increase of the H_2O content in the liquid up to 16% (Table 2, entry 5). Altogether, the comparison of the obtained experimental and modelling results showed the feasibility and applicability of the developed 3D fluid dynamics model for plasma systems.

The results also demonstrated that the amount of the delivered H_2O remained practically the same with and without plasma ignition.

Table 2 Amount of H_2O induced in the liquid D_2O sample after exposure to the COST RF jet operated with various H_2O saturation values of the feed gas and the side flow gas

				H_2O in the liquid sample after exposure[c] (mol%)	
Entry	Feed gas[a]	Side flow gas	Gap[b] (mm)	Ignited plasma	Gas flow without plasma ignition
1	He	—	10	0.7	0.6
2	He with 5% H_2O	—	10	2.3	2.1
3	He with 10% H_2O	—	10	3.6	3.6
4	He with 35% H_2O	—	10	8.9	8.1
5[d]	He with 100% H_2O	—	10	—	16.1
6	He	—	3	0.7	0.7
7	He with 5% H_2O	—	3	2.4	2.6
8	He with 10% H_2O	—	3	3.6	3.6
9	He with 35% H_2O	—	3	8.7	8.4
10	He	He	10	0.8	—
11	He	He with 20% H_2O	10	1.5	—
12	He	He with 100% H_2O	10	2.9	3.2
13	He	He with 100% H_2O	3	0.9	0.8

[a] The He feed gas contained residual humidity even without added water vapour. [b] Distance from the plasma jet nozzle to the liquid surface. [c] Determined by ^{1}H-NMR analysis with an external standard (sodium *p*-toluenesulfonate). [d] Plasma could not be ignited with the 100% H_2O–saturated He feed gas.

It was different from the previously studied parallel field jet, where the delivery of species was significantly enhanced by the ignited plasma.[34] This agrees with the report by Xu *et al.*, where for a cross field and a parallel field plasma jet the authors detect similar production of plasma-produced ROS in the gas phase, but lower ROS concentrations in the liquid for a cross-field jet.[31] This suggests that the enhanced delivery can be ascribed to the presence of an electric field, due to the charged species in the effluent. In their absence (*e.g.*, with the COST RF plasma jet), such effect is not observed. This is an important phenomenon, emphasising the fundamental differences between the cross field and the parallel field plasma jets.

H_2O_2 and OH in the plasma-exposed aqueous samples

In our dedicated reactor with the controlled environment, the only component added to the He gas was H_2O vapour, although the commercial He also contained H_2, O_2 and N_2 impurities, as mentioned in the Modelling section.‡ Under these conditions, the main reactive species to be formed are H, OH and H_2O_2. H and OH radicals are produced by the plasma from the H_2O molecules added to the feed gas, and H_2O_2 is formed through *e.g.* recombination of two OH radicals, as shown in (R.1) and (R.2). We note that these are only representative reactions of the large set of reactions used in the 0D model (see the Computational modelling section). It is thus clear that the amount of H_2O_2 is directly related to the amount of H_2O in the gas phase.

$$e^- + H_2O \rightarrow e^- + OH + H \quad (R.1)$$

$$OH + OH + He \rightarrow H_2O + He \quad (R.2)$$

We performed measurements of the H_2O_2 concentrations in the liquid phase by UV-Vis spectrophotometry with potassium titanium oxide oxalate dihydrate in a mixture of H_2O and H_2SO_4.[10] In the absence of reactive nitrogen species, H_2O_2 is a persistent molecular compound in aqueous solutions,[10,42] so the reagents were added to the exposed liquid after the plasma exposure. The concentration values are quoted after the correction for the evaporated solvent. The temperature measurements showed that the temperature of the aqueous samples did not increase after the plasma exposure. In fact, the temperature of water has decreased from *ca.* 22 °C to 20–21 °C, likely due to the evaporation. Thus, the evaporation of H_2O_2 was disregarded as its vapour pressure is approximately an order of magnitude lower than that of H_2O under experimental conditions.[43] The measured H_2O_2 concentrations in the liquid sample as a function of the H_2O content in the feed gas and in the side flow gas are shown in Fig. 3.

The amount of H_2O_2 was strongly dependent on the feed gas humidity (Fig. 3a). However, the H_2O_2 concentration increased non-linearly with increasing H_2O content of the feed gas. This was likely the result of several factors, such as the lower electron density at high values of molecular admixtures,[44,45] or reactions leading to the loss of H_2O_2.[38] This indicated that H_2O_2 was not formed from the liquid H_2O by electron impact dissociation and subsequent recombination of the OH radicals (see (R.1) and (R.2) above): a lower electron density would result in a lower amount of electrons that reach the liquid, and thus a lower amount of H_2O_2 they could form, while Fig. 3a shows a rising trend. Interestingly, the amounts of H_2O_2 induced in the liquid at 10 and 3 mm were the same. The experimental and modelling data (Tables 2 and 1, respectively) demonstrated that the delivery of species from inside the COST jet into the liquid was also equally efficient at 10 and 3 mm. These data taken together let us hypothesise that H_2O_2 was formed inside the gas phase plasma, and subsequently delivered into the liquid sample by the gas flow.

We compared the experimental results with the computational modelling of the gas phase plasma. The 0D model was used for kinetics simulations of the He plasma with impurities and H_2O admixtures in the feed gas (see Modelling section for details). In this computational model, we looked at the concentrations of H_2O_2, OH and H in the gas phase at different distances from the plasma jet nozzle (3 and 10 mm). The simulations were performed for the gas phase plasma, thus allowing

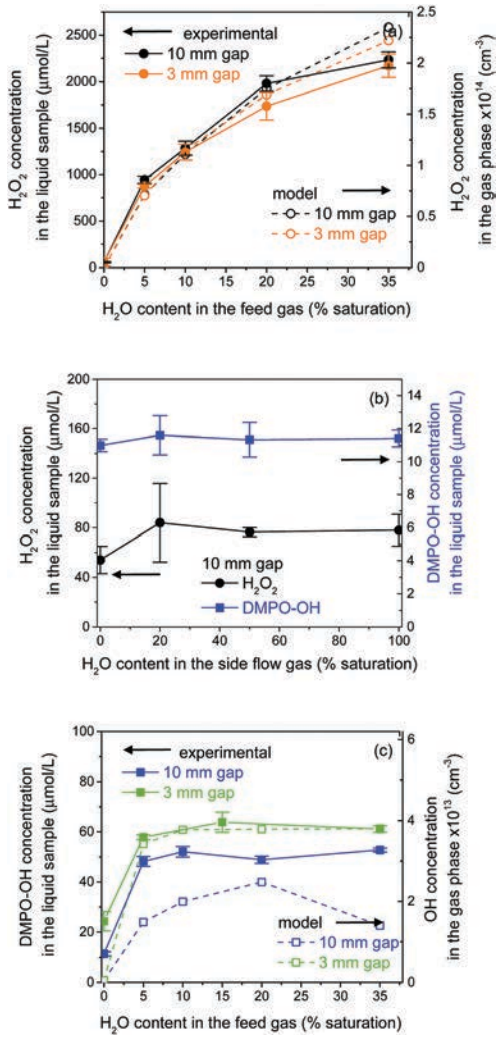

Fig. 3 Measured and calculated concentration of H_2O_2 in the liquid and gas, respectively, for the two different gaps, as a function of feed gas humidity (a); measured H_2O_2 and DMPO-OH concentration in the liquid as a function of the side flow humidity for the 10 mm gap (b); measured DMPO-OH concentration in the liquid and calculated OH concentration in the gas phase as a function of the feed gas humidity for the two different gaps (c). The concentration values of H_2O_2 and OH in the gas phase were obtained from the 0D chemical kinetics computational model. The concentrations of H_2O_2 and DMPO-OH in the liquid were measured by UV-Vis and EPR, respectively.

us to compare the trends, but not the absolute values, of the species formation. A good agreement with the experimental data was observed (dashed lines in Fig. 3a; see also Table S2 in the ESI†). This supported the hypothesis that H_2O_2 is formed in the gas phase and further delivered into the liquid with the gas flow.

Some discrepancy with the model results was, however, that a higher amount of H_2O_2 was detected experimentally in case of the He feed gas with no added water vapour. Here, the amount of H_2O_2 detected in this case in 100 μL of liquid was *ca.* 5×10^{-9} mol, while the computationally predicted value for the gas phase H_2O_2 was in the range of 5×10^{12} L^{-1} (see ESI,† Table S2), corresponding to 8×10^{-12} mol of H_2O_2 formed during 1 min of exposure at 1 L min^{-1}. Furthermore, the amount of H_2O available (during the experiment) was 2×10^{-9} mol, as calculated from the impurities reported in commercial He.‡ The detected amount of H_2O_2 exceeded even the amount of H_2O from the reported impurities. This discrepancy was possibly due to the following reasons. First, the residual humidity in the He feed gas might be higher than the values of the commercial impurities, which are considered in the model, even after an hour of flushing. This is consistent with the elevated amount of H_2O in D_2O after exposure to the 'dry' feed gas (0.6–0.8 mol% as seen in Table 2, entries 1, 6 and 10) compared to that with no gas flow (0.4 mol%; see Experimental, and Table S1 in the ESI†). Second, the model did not include the formation of new reactive species in the effluent from additional water molecules from the evaporated liquid sample. The main pathways leading to the formation of OH (precursor of H_2O_2) are electron impact reactions with H_2O molecules. In a cross field jet such as the COST jet, the amount of electrons in the effluent is minimal and was therefore not included in the model: the charged species were considered to be mostly confined within the jet electrodes. In reality, however, both electrons and other high-energy species may potentially escape the jet (to some extent) and interact with H_2O in the effluent. Nevertheless, except for this discrepancy at dry He feed gas conditions, where the H_2O_2 concentration is anyway low (also in the experiments), the general agreement between experimental and modelling trends is very good.

Although the data of Fig. 3a strongly indicates that H_2O_2 was formed inside the gas phase plasma, and subsequently delivered into the liquid sample by the gas flow, we performed additional experiments to further check the possibility of H_2O_2 formation in the effluent. For this, H_2O vapour was added into the reactor with the side flow of He, while the feed gas He did not contain added water vapour (Fig. 3b). In this case, the humidity in the effluent consisted of the H_2O brought by the side flow gas, and the evaporated liquid sample. While the exact humidity of the gas in the effluent was not calculated due to the unknown mixing rates, we used the fluid dynamics model to estimate the amounts of H_2O diffused into the effluent from the side flow of He, as shown above (Table 1).

The experiments with the side flow gas were only performed with the 10 mm gap between the jet and the liquid, because with the 3 mm gap the diffusion of the H_2O vapour from the side flow into the effluent was very low, as seen from the fluid dynamics model (Table 1), ^{1}H-NMR data (Table 2) and the results of the H atom detection with PBN spin trap in D_2O (*vide infra*). Fig. 3b shows that the concentration of H_2O_2 did not exhibit any significant increase when extra humidity was added to the effluent area. We thus hypothesise that the humidity of the feed gas has a much stronger effect on the amount of H_2O_2 formed.

We assessed the relative contribution of these two plasma compartments (*i.e.*, plasma jet and effluent) as follows. The concentration of H_2O in the effluent with 5% H_2O saturation of the feed gas was predicted by the fluid dynamics model to be *ca.* 50 μmol L^{-1} (Table 1, entry 1). This value is close to the value

predicted for the dry He feed gas and 100% H_2O–saturated side flow (*ca.* 60 μmol L^{-1}; Table 1, entry 7). The ^{1}H-NMR data also showed that the percentage of H_2O brought from the gas into the liquid D_2O sample was similar with 5–10% H_2O–saturation of the feed gas, and with 100% H_2O–saturation of the side flow gas and dry He feed gas (Table 2, entries 2, 3 and 12). However, in spite of the similar H_2O concentrations in the effluent, dramatically less H_2O_2 was produced in case of 100% H_2O saturation of the side flow gas, compared to 5% H_2O saturation of the feed gas: *ca.* 80 μM (Fig. 3b) *vs.* 1000 μM (Fig. 3a). This unambiguously confirms that the humidity of the feed gas affects the formation of H_2O_2 to a much higher extent than the humidity in the effluent. These effects must be considered when tailoring the parameters of the COST RF jet for the production of specific species (*e.g.*, H_2O_2). Furthermore, they also suggest that H_2O_2 is mainly formed inside the COST jet device, rather than in the effluent.

We also investigated the effect of H_2O vapour in the two compartments (*i.e.*, inside the jet and in the effluent) of our plasma system on the formation of the OH radicals. The radicals were detected using the DMPO spin trap, which reacts with the very short-lived radical species to form more persistent radical adducts.[46] In our experiments, the solution of the spin trap was exposed to plasma, and the resulting solution containing the radical adduct was analysed by EPR. We acknowledge that the measured concentration of *e.g.* DMPO-OH radical adduct does not correspond to the absolute amount of the OH radical, because the OH radical can also be lost *via* other reactions (*e.g.*, recombination in the liquid phase). However, as with spin trapping of all plasma-induced species, the trends observed for the DMPO-OH adduct correspond to those of the OH radical.[31,47] We also note that in all cases, DMPO formed adducts with both OH and H radicals (ESI,† Fig. S5). Here, we focus on the DMPO-OH radical adduct, as the spin trapping of the plasma-induced species with DMPO results predominantly in its formation.[34] The effect of the H_2O vapour on the formation of the DMPO-H radical adduct under different experimental conditions can be found in the ESI† (Fig. S6). The effect of the H_2O vapour on the amount of H atoms in the liquid will be discussed further below, with PBN spin trap.

The results of the OH radical spin trapping with DMPO are shown in Fig. 3b and c. The concentration of the DMPO-OH radical adduct in the liquid also increased with increasing humidity of the feed gas, but it flattens out already at 5–10% H_2O saturation of the feed gas (Fig. 3c). In general, the concentration of DMPO-OH formed with the 3 mm gap was higher than with the 10 mm gap. One possible explanation is that the OH radical is formed from the H_2O molecules in the feed gas inside the COST jet. Then, its concentration would decrease at longer gaps due to loss of the radical (*e.g.*, by quenching reaction with H, recombination to form H_2O_2,[22,38] *etc.*). Note that the concentration of H_2O_2 in the liquid could still remain the same, because the OH radical that reached the liquid (at 3 mm) would recombine in the liquid, forming H_2O_2. An alternative explanation includes the formation of OH from additional water molecules in the effluent. This would also lead to a higher concentration of DMPO-OH at 3 mm gap, because more high-energy species are available to form the radicals, which are trapped before they are quenched. However, the introduction of H_2O vapour into the effluent from the side gas flow resulted in only a minor increase in the DMPO-OH concentration (Fig. 3b), indicating that most of the OH radicals were not formed in the effluent.

The trends observed experimentally compared rather well with those predicted by the model for the OH radical in the gas phase (Fig. 3c). Although the difference between the 3 and 10 mm gaps is larger in the computational model, and the calculation results at 10 mm gap exhibit a somewhat different trend, the predicted trends were in general agreement with the experimental data. Like for H_2O_2, a discrepancy with the model was observed when increasing the H_2O content of the feed gas from 0 to 5%. With the 'dry' He feed gas, the high concentration (compared to the feed gas with 5% H_2O) of DMPO-OH was possibly due to the high residual humidity (see above).

Altogether, our results are in good agreement with previously obtained results for a parallel field kHz plasma jet.[34] The H_2O_2 was shown to be largely formed in the gas phase inside the jet. However, in the present study with the COST RF plasma jet, we propose that the OH radicals were also mostly formed inside the plasma jet, with minor amounts formed in the effluent. We attribute this difference to the absence of electrons in the effluent, in contrast to a parallel field kHz plasma jet.

H radical induced in the plasma-exposed aqueous samples

The use of the isotopically labelled water enables discrimination between the H radicals (atoms) formed from the gas phase water and water from the liquid sample. The trapping of the H radicals was performed by exposing solutions of the PBN spin trap in H_2O to the plasma jet. Unlike DMPO, PBN reacted predominantly with H radicals, forming PBN-H radical adducts (see Fig. S7 in the ESI†). Our initial results showed that the presence of oxygen in the effluent has a detrimental effect on the amount of the trapped H radicals (ESI,† Fig. S8). This was likely due to the quenching of H *via* reactions[23,38] with O_2 or O,[29,47] and confirmed the requirement for the use of the glass reactor in our experiments.

We investigated the effect of the water vapour saturation of the feed gas on the formation of the PBN radical adducts in the liquid under two conditions: PBN was dissolved in H_2O and D_2O, and the feed gas was saturated with H_2O or D_2O vapour (Fig. 4). Using two different water molecules, H_2O and D_2O, we were able to distinguish between the radicals formed from the gas phase and the liquid phase water.

First, solutions of PBN in H_2O and D_2O were exposed to plasma (Fig. 4). At the 3 mm gap between the jet and the liquid sample, the concentration of PBN-H was higher than at 10 mm (Fig. 4a and b), as was also the case with the DMPO-OH spin trapping (Fig. 3). However, the concentration of PBN-H formed in H_2O when exposed to plasma with different H_2O contents in the feed gas did not change significantly. Indeed, they remained at *ca.* 14 and 20 μmol L^{-1} for the gaps of 10 and 3 mm, respectively, for all values of the feed gas humidity (Fig. 4a). The trends of

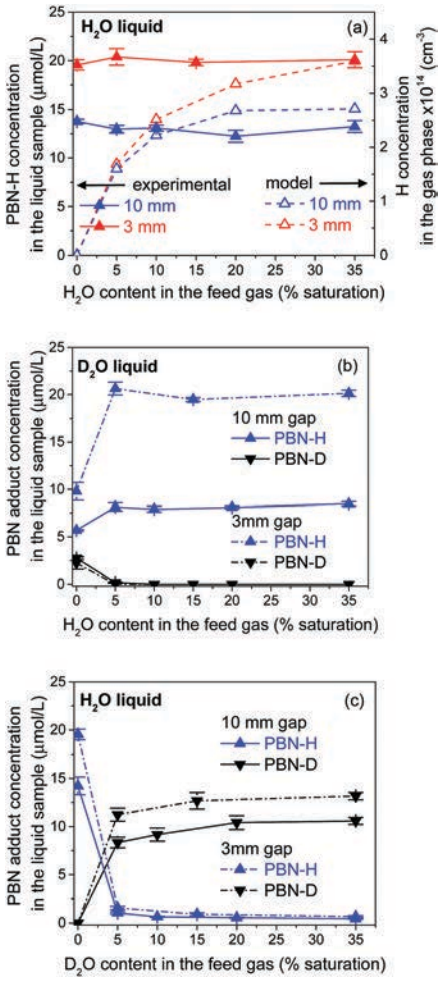

Fig. 4 Measured concentration of the PBN radical adducts in the liquid, as a function of the feed gas humidity, for the two different gaps. Plasma exposure conditions: H_2O liquid, H_2O in the feed gas (a); D_2O liquid, H_2O in the feed gas (b); H_2O liquid, D_2O in the feed gas (c). In (a) the calculated concentration (density) of H in the gas phase, obtained with a 0D chemical kinetics computational model is plotted as well. The concentrations of PBN-H and PBN-D were measured by EPR.

H density in the gas phase predicted by the 0D model (dashed lines in Fig. 4a) only agree to some extent with the experimental results, regarding the existing difference between the 10 mm and 3 mm gap. However, the calculated values clearly rose with higher H_2O content in the feed gas while the measured values were nearly constant. In other words, the experimental results showed unexpectedly high concentrations of PBN-H for the conditions with lower percentage of water (0–10% H_2O saturation of the feed gas). The reason for this might be the residual humidity in the feed gas, as was shown for DMPO-OH and H_2O_2. Alternatively, it is possible that these unexpectedly large amounts of H radicals were formed from the H_2 impurities in the feed gas,[34] which could be higher than the supplier's specification.

Further, PBN in liquid D_2O was exposed to plasma with the H_2O-containing He feed gas (Fig. 4b). Only the H radical was trapped with 5% H_2O saturation of He and above, as is clearly seen from the figure. With no added H_2O vapour, both PBN-H and PBN-D radical adducts were formed. This means that both H_2O (from the residual humidity in the feed gas) and D_2O (from the liquid sample) are involved in the formation of the radicals. Moreover, with this 'dry' He, more PBN-H was formed with the 3 mm gap than with 10 mm (*ca.* 10 and 6 μM, respectively). This suggests that some H radicals must indeed originate in the gas phase plasma inside the COST jet, and with the larger gap they undergo quenching before they reach the liquid sample. As a control experiment to confirm that H was not formed from the possible residual H_2O in the reactor, we flushed the closed reactor with He for approximately 3 h. The D_2O sample with PBN was then injected into the reactor using a syringe. This extensive flushing did not increase the D/H ratio of the trapped radicals (ESI,† Table S3), confirming that the H radicals originated from the residual, yet high, humidity in the feed gas.

As mentioned above, only for dry He feed gas, some PBN-D adduct was detected (not exceeding 30% of the total amount of both PBN adducts; Fig. 4b). It can be formed either from the evaporated D_2O sample, or from the liquid D_2O. When no H_2O vapour was added to the He feed gas, the liquid D_2O sample contained less than 1 mol% H_2O (as can be deduced from Table 2). Still, more PBN-H adduct than PBN-D adduct was formed in the liquid (Fig. 4b), suggesting that the radicals were not formed in the liquid. The same can be concluded from the fact that the concentration of PBN-H does not decrease with the increased humidity of the feed gas (*i.e.*, decreased electron density). However, another factor also influenced the distribution of the radicals detected: the primary kinetic isotope effect (KIE) in the formation of H and D radicals from H_2O and D_2O molecules. We assessed the value of the KIE in our experiments as follows. The feed gas saturation with water was 35% to minimise the effect of the residual humidity. This 35% saturation in turn consisted of various ratios of H_2O/D_2O (achieved by mixing various amounts of H_2O/D_2O in a Drechsel flask with passing He). The liquid sample consisted of the same H_2O/D_2O ratio as the feed gas humidity. This way, the empirical KIE value did not depend on whether the radicals are formed in the liquid or in the gas phase. Table 3 shows the effect of the KIE. For example, with the 1 : 9 ratio of H_2O/D_2O in the plasma system

Table 3 Experimental values of the KIE obtained from the distribution of PBN-H and PBN-D radical adducts formed in a liquid sample

	Isotopic distribution in the gas and the liquid[a] (mol%)		Radical adduct detected in the liquid[b] (%)		
Entry	H_2O	D_2O	PBN-H	PBN-D	KIE[c]
1	5	95	13	87	2.8
2	10	90	26	74	3.1
3	20	80	43	57	3.0
4	30	70	59	41	3.3
5	40	60	65	35	2.8
				Avg.	3.0

[a] Achieved by mixing H_2O/D_2O in the Drechsel flask with passing He in the same proportion as the liquid sample. Total water saturation of He was 35%. [b] Determined by EPR analysis. The presented values are averaged over three experiments. [c] Calculated as shown in eqn (5).

(both gas and liquid), the ratio of formed H and D radical adducts detected in the liquid was 26 : 74 (Table 3, entry 2). Similar trends are seen for the other H_2O/D_2O ratios in the plasma system (see other conditions of Table 3). Averaged over the various conditions, the found value of KIE (calculated as shown in eqn (4)) was 3.0, as seen in the last column in Table 3. This value was in complete agreement with our previous work with the parallel-field plasma jet.[34] These results suggest that the radicals detected in the liquid were not formed from the liquid water molecules. Indeed, if they were, PBN-D would be the major product, even with the KIE taken into account. For example, consider an experiment with a solution of PBN in D_2O exposed to the plasma with 35% H_2O–saturated feed gas. After the exposure, the H_2O content in the liquid D_2O was *ca.* 8–9% (as shown in Table 2; entry 4). Let us assume that the radicals were formed in the liquid sample. Then, using eqn (5) and the found KIE value of 3.0, we get a ratio of PBN-D/PBN-H of 3.37. This would correspond to *ca.* 77% of PBN-D and 23% of PBN-H, which was clearly not the case (Fig. 4b), again indicating that these radicals were not formed in the liquid.

$$\mathrm{KIE} = \frac{\%_{\text{PBN-H}} \cdot \mathrm{mol}\%_{D_2O}}{\%_{\text{PBN-D}} \cdot \mathrm{mol}\%_{H_2O}} \quad (5)$$

Similar effects were observed when PBN in H_2O was exposed to the plasma with feed gas containing D_2O vapour. With as little as 5% D_2O vapour in the feed gas, predominantly PBN-D was detected in the liquid sample (Fig. 4c), in agreement with the results of D_2O liquid and H_2O vapour. These data combined unambiguously show that the H and D radicals detected in the liquid were not formed from the liquid water molecules, but originated from the gas phase water. Finally, the fourth combination, *i.e.*, the D_2O liquid and D_2O vapour system, was also investigated. The results show that at 10 mm, only D radicals were detected, while at 3 mm some H was still seen (see ESI,† Fig. S9), again attributed to the residual humidity in the feed gas. This was possibly due to quenching of the H radicals in the effluent at the longer gap.

The effect of the effluent composition was studied by exposing PBN in D_2O to the dry He feed gas plasma with added side flow H_2O vapour. The results are plotted in Fig. 5. With the 3 mm gap, virtually no changes in the concentrations of the trapped H and D radicals were observed (Fig. 5a). This was due to the minimal diffusion of the side flow gas components into the effluent, as also seen from the results of the ^{1}H-NMR analysis of the composition of the liquid D_2O samples, as well as the 3D fluid dynamics model results (see above). However, the 10 mm gap showed an increase of the trapped H radicals (from *ca.* 6 to 8 μM) and a decrease in the D radicals (from 3 to 1 μM).

A similar effect is seen for the inversed conditions, when PBN was in liquid H_2O, and D_2O vapour was introduced into the effluent from the side gas flow (Fig. 5b). There are two possible explanations. First, the H and D radicals could be formed in the effluent by *e.g.* electron impact reactions from the H_2O (evaporated sample) and D_2O (side flow gas) molecules. At the same time, the D_2O/H_2O composition changes towards higher amounts of D_2O as added vapour is coming into

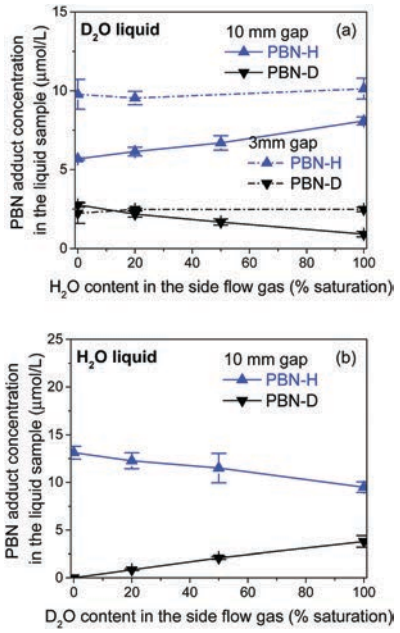

Fig. 5 Concentration of the PBN radical adducts in the liquid as a function of the side flow gas humidity. Plasma exposure conditions: D_2O liquid, H_2O in the side flow gas (a); H_2O liquid, D_2O in the side flow gas (b).

the effluent from the side flow gas. This, however, assumes that radicals are formed in the effluent, which is not supported by our other observations (see DMPO-OH). The second explanation involves the formation of H radicals inside the plasma jet from *e.g.* residual humidity (the high amount of H radicals was shown to be inherent to the feed gas, see Fig. 4). These H radicals can further interact with the D_2O molecules in the effluent, creating D radicals (R.3). This can explain why the PBN-D adduct concentration rises and the PBN-H adduct concentration drops upon higher D_2O content in the side flow (Fig. 5b).

$$D_2O + H \rightarrow HOD + D \quad (R.3)$$

In the opposite case (Fig. 5a), the liquid D_2O sample evaporates, adding D_2O vapour to the effluent. In the absence of the side flow gas, the H radicals are formed inside the plasma jet, and then interact with D_2O (R.3). This explains the 30% of the PBN-D adduct detected with the 'dry' He feed gas (Fig. 4b and 5a). As the side flow gas brings more H_2O vapour, the D_2O/H_2O vapour ratio in the effluent decreases. Thus, fewer of the H radicals formed in the jet react with D_2O in the effluent because of its lower relative amount. This decreases the number of the D radicals. *Vice versa*, the amount of H radicals is higher because (R.3) occurs to a lower extent.

We believe that this second explanation is more feasible. Indeed, when PBN was in liquid H_2O and H_2O vapour was introduced in the side flow gas, the amount of the trapped PBN-H did not increase upon higher H_2O content in the effluent (ESI,† Fig. S10). This supports the hypothesis that the reaction (R.3) takes place, and that H radicals, like OH and H_2O_2, mostly originate in the plasma inside the jet.

Conclusions

The COST RF plasma jet is a standard reference jet, developed within an EU COST action with the purpose to be used in low temperature atmospheric plasma research. Its biomedical activity, such as the deactivation of cancer cells, sterilisation and wound healing, is governed by the formation of reactive species. In this work we investigated the origin of the reactive species induced in aqueous solutions exposed to the COST jet. For the first time, experimental analytical techniques (EPR, UV-Vis, ^{1}H-NMR) were combined with a 0D chemical kinetics model and a 3D fluid dynamics model to elucidate in which reactive compartment (*i.e.*, inside plasma jet, plasma effluent or liquid) the reactive species detected in the liquid are formed. The study was performed in a dedicated reactor which encapsulated the jet to control the atmosphere in the plasma effluent. This allowed a controlled humidity in the effluent by adding water vapour with the side flow gas inside the reactor. We studied the effect of the feed gas humidity and the humidity in the effluent on the concentrations of the radical adducts DMPO-OH and PBN-H, as well as the H_2O_2 concentration, in the liquid solution. We compared the experimental trends of the concentrations of the detected species with the trends of H_2O_2, OH and H densities predicted by the computational model for the gas phase plasma for different plasma conditions. The use of isotopically labelled water and EPR analysis in conjunction with ^{1}H-NMR allowed distinguishing between the radicals formed from the feed gas (or side flow gas) water and from the evaporated sample.

The presented results demonstrate that all studied species originated from the gas phase. Moreover, we propose that they were formed mostly inside the plasma jet from the feed gas admixtures, while minor amounts are formed from the effluent humidity. In the plasma effluent, further reactions take place, without significant amounts of new species formed. This makes the COST RF plasma jet fundamentally different from a parallel field plasma jet system, in which, as we reported previously, radical species were formed exclusively in the plasma effluent. This study provides important insights into the reactive compartments of the COST jet in contact with aqueous solutions. It adds to the overall understanding of the chemistry induced in liquids by the COST RF plasma jet, and can aid in further research on its applications.

Conflicts of interest

There are no conflicts to declare.

Acknowledgements

We are grateful to Volker Schulz-von der Gathen (Experimental Physics II: Application Oriented Plasma Physics, Ruhr-Universität Bochum, Germany) for providing the COST RF plasma jet. We thank our colleagues at the University of Antwerp: Gilles Van Loon (Mechanical Workshop), Karen Leyssens (Research group PLASMANT), and Sylvia Dewilde (Department of Biomedical Sciences) for their help with the equipment. This work was funded by the European Marie Sklodowska-Curie Individual Fellowship 'LTPAM' within Horizon2020 (grant no. 657304). Stefan Tinck thanks the Fund for Scientific Research – Flanders (FWO) for supporting his work (grant no. 0880.212.840).

Notes and references

1 X. Lu, G. V. Naidis, M. Laroussi, S. Reuter, D. B. Graves and K. Ostrikov, *Phys. Rep.*, 2016, **630**, 1.
2 K.-D. Weltmann and Th. von Woedtke, *Plasma Phys. Controlled Fusion*, 2017, **59**, 014031.
3 I. Adamovich, S. D. Baalrud, A. Bogaerts, P. J. Bruggeman, M. Cappelli, V. Colombo, U. Czarnetzki, U. Ebert, J. G. Eden and P. Favia, *et al.*, *J. Phys. D: Appl. Phys.*, 2017, **50**, 323001.
4 M. Yoshinari, K. Matsuzaka and T. Inoue, *Jpn. Dent. Sci. Rev.*, 2011, **47**, 89.
5 K. Bazaka, M. V. Jacob, W. Chrzanowski and K. Ostrikov, *RSC Adv.*, 2015, **5**, 48739.
6 V. Arora, V. Nikhil, N. K. Suri and P. Arora, *Dentistry*, 2014, **4**, 1.
7 H. Shintani and A. Sakudo, *Gas Plasma Sterilization in Microbiology: Theory, Applications, Pitfalls and New Perspectives*, Caister Academic Press, Poole, 2016.
8 A. Privat-Maldonado, Y. Gorbanev, D. O'Connell, R. Vann, V. Chechik and M. W. van der Woude, *IEEE Trans. Radiat. Plasma Med. Sci.*, 2017, DOI: 10.1109/TRPMS.2017.2761405.
9 H. A. Aboubakr, U. Gangal, M. M. Youssef, S. M. Goyal and P. J. Bruggeman, *J. Phys. D: Appl. Phys.*, 2016, **49**, 204001.
10 W. Van Boxem, J. Van der Paal, Y. Gorbanev, S. Vanuytsel, E. Smits, S. Dewilde and A. Bogaerts, *Sci. Rep.*, 2017, **7**, 16478.
11 S. Vermeylen, J. De Waele, S. Vanuytsel, J. De Backer, J. Van der Paal, M. Ramakers, K. Leyssens, E. Marcq, J. Van Audenaerde, E. L. J. Smits, S. Dewilde and A. Bogaerts, *Plasma Processes Polym.*, 2016, **13**, 1195.
12 D. Yan, J. H. Sherman and M. Keidar, *Oncotarget*, 2017, **8**, 15977.
13 S. Bekeschus, A. Schmidt, K.-D. Weltmann and Th. von Woedtke, *Clin. Plasma Med.*, 2016, **4**, 19.
14 G. Y. Park, S. J. Park, M. Y. Choi, I. G. Koo, J. H. Byun, J. W. Hong, J. Y. Sim, G. J. Collins and J. K. Lee, *Plasma Sources Sci. Technol.*, 2012, **21**, 043001.
15 D. B. Graves, *Phys. Plasmas*, 2014, **21**, 080901.
16 X. Lu, M. Laroussi and V. Puech, *Plasma Sources Sci. Technol.*, 2012, **21**, 034005.
17 D. Xiao, C. Cheng, J. Shen, Y. Lan, H. Xie, X. Shu, Y. Meng, J. Li and P. K. Chu, *J. Appl. Phys.*, 2014, **115**, 033303.
18 Y. Gorbanev, D. Leifert, A. Studer, D. O'Connell and V. Chechik, *Chem. Commun.*, 2017, **53**, 3685.
19 J. Golda, J. Held, B. Redeker, M. Konkowski, P. Beijer, A. Sobota, G. Kroesen, N. St. J. Braithwaite, S. Reuter and M. M. Turner, *J. Phys. D: Appl. Phys.*, 2016, **49**, 084003.
20 B. Barwe, F. Riedel, O. Cibulka and J. Benedikt, *J. Phys. D: Appl. Phys.*, 2015, **48**, 314001.
21 A. West, M. van der Schans, C. Xu, M. Cooke and E. Wagenaars, *Plasma Sources Sci. Technol.*, 2016, **25**, 02LT01.

22 T. Murakami, K. Niemi, T. Gans and D. O'Connell, *Plasma Sources Sci. Technol.*, 2013, **22**, 15003.
23 T. Murakami, K. Niemi, T. Gans, D. O'Connell and W. G. Graham, *Plasma Sources Sci. Technol.*, 2014, **23**, 025005.
24 N. Knake, K. Niemi, S. Reuter, V. Schulz-von der Gathen and J. Winter, *Appl. Phys. Lett.*, 2008, **93**, 131503.
25 A. Wijaikhum, D. Schröder, S. Schröter, A. R. Gibson, K. Niemi, J. Friderich, A. Greb, V. Schulz-von der Gathen, D. O'Connell and T. Gans, *Plasma Sources Sci. Technol.*, 2017, **26**, 115004.
26 J. Benedikt, D. Schröder, S. Schneider, G. Willems, A. Pajdarová, J. Vlček and V. Schulz-von der Gathen, *Plasma Sources Sci. Technol.*, 2016, **25**, 045013.
27 S. Große-Kreul, S. Hübner, S. Schneider, D. Ellerweg, A. von Keudell, S. Matejčík and J. Benedikt, *Plasma Sources Sci. Technol.*, 2015, **2**, 044008.
28 K. Wende, P. Williams, J. Dalluge, W. Van Gaens, H. Aboubakr, J. Bischof, T. von Woedtke, S. M. Goyal, K.-D. Weltmann, A. Bogaerts, K. Masur and P. J. Bruggeman, *Biointerphases*, 2015, **10**, 029518.
29 M. M. Hefny, C. Pattyn, P. Lukes and J. Benedikt, *J. Phys. D: Appl. Phys.*, 2016, **49**, 404002.
30 T. Takamatsu, K. Uehara, Y. Sasaki, H. Miyahara, Y. Matsumura, A. Iwasawa, N. Ito, T. Azuma, M. Kohno and A. Okino, *RSC Adv.*, 2014, **4**, 39901.
31 H. Xu, C. Chen, D. Liu, D. Xu, Z. Liu, X. Wang and M. G. Kong, *J. Phys. D: Appl. Phys.*, 2017, **50**, 245201.
32 J. Winter, H. Tresp, M. U. Hammer, S. Iseni, S. Kupsch, A. Schmidt-Bleker, K. Wende, M. Dünnbier, K. Masur and K.-D. Weltmann, *J. Phys. D: Appl. Phys.*, 2014, **47**, 285401.
33 C. C. W. Verlackt, E. C. Neyts and A. Bogaerts, *J. Phys. D: Appl. Phys.*, 2017, **50**, 11LT01.
34 Y. Gorbanev, D. O'Connell and V. Chechik, *Chem. – Eur. J.*, 2016, **22**, 3496.
35 Spin Trap Database, National Institute of Environmental Health Sciences, available online at: http://tools.niehs.nih.gov/stdb/.
36 Y. Gorbanev, N. Stehling, D. O'Connell and V. Chechik, *Plasma Sources Sci. Technol.*, 2016, **25**, 055017.
37 S. Pancheshnyi, presented in part at the 61st Annual Gaseous Electronics Conference, Dallas, October-2008.
38 V. Van Gaens and A. Bogaerts, *J. Phys. D: Appl. Phys.*, 2013, **46**, 275201.
39 G. J. M. Hagelaar and L. Pitchford, *Plasma Sources Sci. Technol.*, 2005, **14**, 722.
40 S. Kelly, J. Golda, M. M. Turner and V. Schulz-von der Gathen, *J. Phys. D: Appl. Phys.*, 2015, **48**, 444002.
41 Y. Gorbanev, R. Soriano, D. O'Connell and V. Chechik, *J. Visualized Exp.*, 2016, **117**, e54765.
42 C. N. Satterfield and A. H. Bonnell, *Anal. Chem.*, 1955, **27**, 1174.
43 D. R. Lide, *CRC Handbook of Chemistry and Physics*, CRC Press, Boca Raton, 1992.
44 A. Fridman, *Plasma Chemistry*, Cambridge University Press, New York, 2012.
45 A. Schmidt-Bleker, J. Winter, A. Bösel, S. Reuter and K.-D. Weltmann, *Plasma Sources Sci. Technol.*, 2015, **25**, 015005.
46 M. Kohno, *J. Clin. Biochem. Nutr.*, 2010, **47**, 1.
47 D. T. Elg, I.-W. Yang and D. B. Graves, *J. Phys. D: Appl. Phys.*, 2017, **50**, 475201.

